Journal of Applied Fluid Mechanics, Vol. 16, No.1, pp. 21-33, 2023.
Available online at www.jafmonline.net, ISSN 1735-3572, EISSN 1735-3645.
https://doi.org/10.47176/jafm.16.01.1382

Numerical Investigations on the Fluid Behavior in the Near Wake of an Experimental Wind Turbine Model in the Presence of the Nacelle

A. Bouhelal[1†], A. Smaili[1], O. Guerri[2] and C. Masson[3]

[1] *Laboratory of Green and Mechanical Development (LGMD), École Nationale Polytechnique, B.P. 182, El-Harrach, Algiers, 16200, Algeria*
[2] *Renewable Energy Development Center (CDER), B.P. 62, Route de l'Observatoire, Bouzaréah, Algiers, Algeria*
[3] *Department of Mechanical Engineering, École de Technologie Supérieure, 1100 Notre-Dame Ouest, H3C1K3, Montréal, Québec, Canada*

†*Corresponding Author Email: abdelhamid.bouhelal@g.enp.edu.dz*

(Received June 16, 2022; accepted August 16, 2022)

ABSTRACT

Accurate predictions of the near wake of horizontal-axis wind turbines are critical in estimating and optimizing the energy production of wind farms. Consequently, accurate aerodynamic models of an isolated wind turbine are required. In this paper, the steady-state flow around an experimental horizontal-axis wind turbine (known as the MEXICO model) is investigated using full-geometry computational fluid dynamics (CFD) simulations. The simulations are performed using Reynolds-Averaged Navier-Stokes (RANS) equations in combination with the transitional k-kl-ω turbulence model. The multiple reference frame (MRF) approach is used to allow the rotation of the blades. The impacts of the nacelle and blade rotation on the induction region and near wake are highlighted. Simulation cases under attached and detached flow conditions with and without the nacelle were compared to the detailed particle image velocimetry (PIV) measurements. The axial and radial flow behaviors at the induction region have been analyzed in detail. This study attempts to highlight the nacelle effects on the near wake flow and on numerical prediction accuracy under various conditions, as well as the possible reasons for these effects. According to simulation results, the rotation of blades dominates the near wake region, and including the nacelle geometry can improve both axial and radial flow prediction accuracy by up to 15% at high wind speeds. At low wind speeds, the nacelle effects can be ignored. The presence of the nacelle has also been shown to increase flow separation at the trailing edges of the blade airfoils, increasing both root and tip vorticities. Finally, small nacelle diameters are recommended to reduce flow separation on the blades and increase the average velocity downstream of the rotor, thereby optimizing wind farm output power.

Keywords: Wind turbine; Aerodynamics; Near wake; Nacelle-blade interaction; CFD; Mexico.

NOMENCLATURE

C_f	skin friction coefficient
$\vec{V}$	velocity vector
$\bar{p}$	average pressure
$\bar{u}$	average axial velocity
u_∞	freestream wind speed
u_τ	friction velocity
$\bar{w}$	average tangential velocity
y^+	dimensionless wall distance
y_p	first mesh element near the wall
D	rotor diameter
F_N	normal force
k	turbulence kinetic energy
kl	laminar kinetic energy
Re	Reynolds number
TSR	Tip Speed Ratio
ω	inverse turbulent time scale
x,y,z	cartesian coordinates
$\bar{v}$	average radial velocity
S_ϕ	source term
$\vec{\nabla}$	Nabla operator
τ_w	wall shear stress
μ	dynamic viscosity
ρ	fluid density
Γ	diffusion coefficient
ϕ	general transport variable

1. INTRODUCTION

Due to the increasing demand for energy, especially clean energy, wind turbines are usually installed in large arrays or grids known as wind farms. In a wind farm, wind turbines can be placed in the wake of upstream turbines, producing 40% to 60% less power than in isolated conditions (Santoni *et al*. 2017). Therefore, accurately predicting the wake of an isolated wind turbine leads to good estimation and optimization of the wind farm's overall power production.

The wake developing downstream of a wind turbine can be divided into two regions: the near wake and the far wake. The far wake is located far from the wind turbine and immediately impacts the downstream turbines. The near wake is an induction region located downstream of a wind turbine at a distance of 1 to 5 times the rotor diameter (Abraham *et al*. 2019).

Accurate predictions of the near wake are critical in many onshore and offshore wind turbine applications, including but not limited to the following:

(i) Develop and improve fast engineering wake models (Bastankhah and Porté-Agel 2014; Madsen and Rasmussen 2004);

(ii) Increase the accuracy of the nacelle anemometry technology (Dahlberg *et al*. 1999; Smaili and Masson 2004), which is used as a practical way to estimate the wind farm output power;

(iii) Evaluate the available annual energy production in a given site (Feng *et al*. 2018);

(iv) Control and optimization of wind farms (Bartl and Sætran 2016);

(v) Optimize the aerodynamics-hydrodynamics interaction for offshore wind turbines (Gao *et al*. 2022);

(vi) Evaluate the maintenance testing and safety of wind turbine systems (Thomsen *et al*. 2007).

Different numerical methods are used to predict the near wake flow downstream of wind turbines, including the free/fixed vortex wake models (Sanderse *et al*. 2011; Tescione *et al*. 2016), actuator disc/surface/line models (De Cillis *et al*. 2021; Z. Gao *et al*., 2021; Masson and Smaili 2006; Masson *et al*. 2001; Sørensen *et al*. 1998) and the full-geometry CFD (computational fluid dynamics) model (Bouhelal *et al*. 2018; Sørensen *et al*. 2002). The full-geometry CFD model is thought to be more accurate than other methods because it does not require rotor data, unlike actuator disc/surface/line and vortex models (Hansen *et al*. 2006).

The geometry of the wind turbine, such as blades, nacelle, and tower, is responsible for the development of the near wake. To differing degrees, all these components (i.e., blades, nacelle, and tower), with their interactions with the fluid, contribute to the formation of the wake. Based on full-geometry CFD simulations, Zahle and Sørensen (2008) investigated the influence of the tower on the wake of a multi-megawatt wind turbine model. The nacelle and tower are found to create important quantities of turbulence in the near wake, considerably increasing the turbulent kinetic energy. The tower effect has been shown to have the least influence on the development of the wake. In comparison to the effect of the nacelle, the effect of the tower can be ignored. The same conclusion has been also demonstrated for small-scale wind turbines (Guo *et al*. 2021; Santoni *et al*. 2017).

Numerous studies have been carried out in order to better understand the role of the nacelle in the development of the near wake downstream of wind turbines. Micallef *et al*. (2013) demonstrated that radial flow dominates near wake flows and its complicated behavior is affected only by the blade geometry (Akay *et al*. 2014).

Many studies have shown that the nacelle effect is caused by flow separation in the rotor's root region and the formation of root vortices. Weihing *et al*. (2018) showed that increasing the diameter of the nacelle reduces the performance of the rotor at the root and increases flow separation.

Abraham *et al*. (2019) observed, using an experimental study, that the turbulent kinetic energy field enhances turbulence in locations of high shear behind the blade tips and nacelle, and decreases turbulence behind the tower. Based on large eddy simulations, Zhu *et al*. (2022) concluded that the nacelle and tower increase the instability of the tip vortices.

Guo *et al*. (2021) showed that the increase in vorticities and turbulent kinetic energy produced by a wind turbine in the presence of a nacelle is the primary cause of rotor output power fluctuations. These fluctuations lead to an increase in fatigue loads and thus reduce wind turbine life operation.

It has been proven from the literature that both steady (Bouhelal *et al*. 2018) and unsteady (Regodeseves and Morros 2021) full-geometry CFD simulations produce good predictions of aerodynamic performance and velocities in the near wake. For both cases, the Reynolds-Averaged Navier-Stokes (RANS) approach is widely used for turbulence modeling. Sørensen *et al*. (2016) investigated the transition effects in RANS turbulence models, and it has been demonstrated that the transition effects can improve the accuracy of the predictions.

Reliable experimental measurements are required to validate numerical wake models. The measurements carried out in Europe's largest wind tunnel under a project known as MEXICO (Model rotor EXperiments In COntrolled conditions) (Boorsma and Schepers 2014; Snel *et al*. 2007) are probably the most widely used among researchers. The MEXICO project provides measurements of aerodynamics and velocities in the wake under various conditions.

From the literature, the nacelle modeling leads to an improvement in the wake prediction accuracy. However, the magnitude of this improvement and its relation to the tip speed ratio (TSR) are not well

understood. This research advances our understanding of the physics of near wake flows downstream of wind turbines. It also aims to investigate the fluid flow features in the induction region by quantifying the effect of blade rotations in the presence of the nacelle. For this purpose, a full-geometry CFD model has been proposed to simulate the steady-state flow around the MEXICO wind turbine using a transitional turbulence model (namely the k-kl-ω turbulence model).

In order to investigate the effect of the nacelle on the near wake downstream of the MEXICO wind turbine, simulated flow at attached and detached conditions with and without the nacelle was compared to detailed PIV measurements for different TSR (varying from 4 to 10).

The following questions are addressed in this study: (i) to what extent can the presence of the nacelle affect the evolution of the fluid behind the rotor and thus the accuracy of the near wake predictions? (ii) how does this effect relate to TSR? The investigation also looks into the possible causes of the nacelle effect by analyzing the axial and radial behavior of the flow, as well as the flow separation in the blade under various conditions.

The following sections highlight the MEXICO wind turbine model, PIV measurements, numerical method, and simulation results.

2. EXPERIMENTAL DESCRIPTION

In this study, the MEXICO wind turbine model was used since it provides experimental data for wind speeds in the near wake. The data is provided through the MexNext project's collaboration (Boorsma and Schepers 2014). The measurements were carried out in the German Dutch wind tunnels in 2014.

2.1 Wind turbine Model Description

MEXICO is a three-bladed, upwind, pitch control wind turbine. The diameter of the rotor is 4.5 m, while the height of the tower is 5.12 m. MEXICO model is characterized by a huge nacelle, measuring 4.4 m in length and 0.54 m in diameter. The blade geometry was created using three different airfoils (see Fig. 1). The blades are twisted and have a non-uniform chord (see Fig. 2).

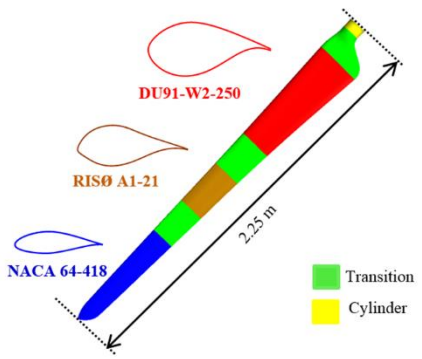

Fig. 1. Geometry of the MEXICO blade.

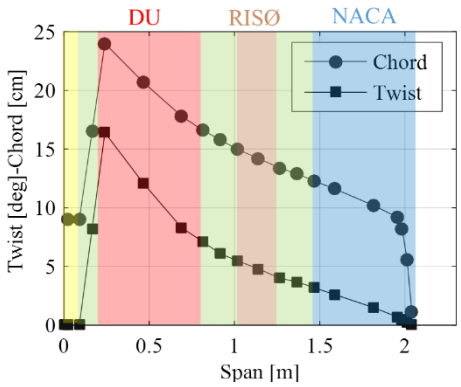

Fig. 2. Distributions of the chord and the twist along the MEXICO blade span.

2.2 Test Cases Description

Three axial upstream wind speeds have been tested, including low speed (TSR = 10), design speed (TSR = 6.7), and flow separation speed (TSR = 4). Particle Image Velocimetry (PIV) stereos were used to measure the axial and radial velocities components in three directions (x, y, and z) in the near wake at the 9 o'clock horizontal plane.

Velocity profiles were measured in different axial and radial transverse positions as shown in Fig. 3. The axial lines cover a distance of 10 m from upstream to downstream, whereas the radial lines cover about 3 m in the near wake. In addition, about 150 dynamic pressure sensors have been used to measure the rotor loads. For more detail, see (Boorsma and Schepers 2014; Schepers *et al.* 2014).

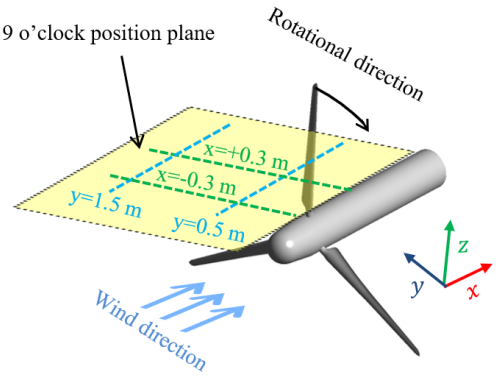

Fig. 3. An overview of the near wake measurement lines of the MEXICO wind turbine.

3. NUMERICAL METHOD

3.1 Computational Domain

Two computational domain configurations have been created with and without the nacelle using the ANSYS DesignModeler tool to investigate the effect of the nacelle on the near wake. The first configuration includes the entire rotor geometry (i.e., blades, hub, and nacelle), whereas the second is a reduced configuration that only includes an isolated blade. The second configuration thus represents one-

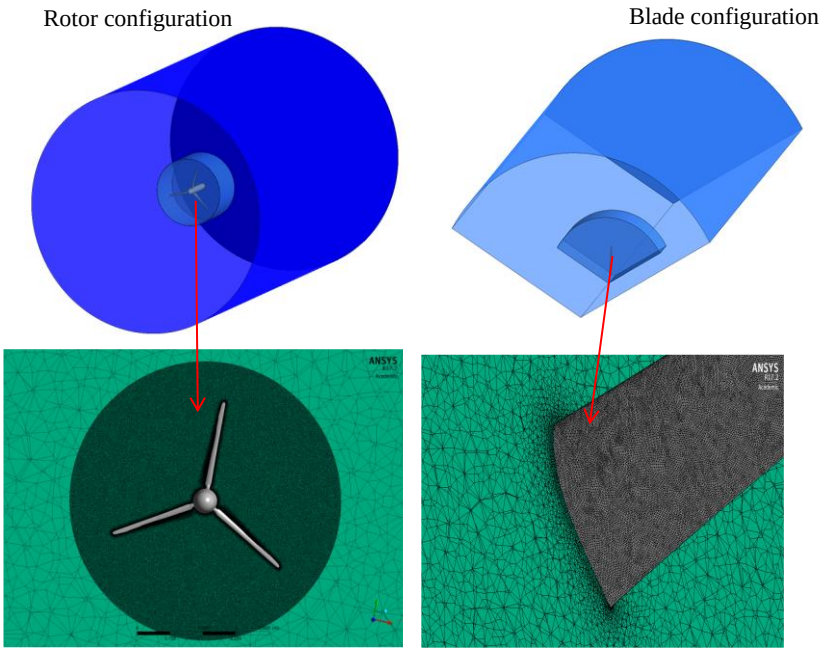

Fig. 4. Computational domain and mesh for the two studied configurations: Rotor (with the nacelle) and Blade (without the nacelle).

third of the full configuration. In the rest of this paper, these two configurations will be referred to as "Rotor" and "Blade" configurations respectively.

The computational domain, for both configurations, represents a cylinder 7.5×D in length and 5×D in diameter, where D is the rotor diameter. Cylindrical configurations were created around the blade and rotor in order to separate the rotating domain from the stationary domain and to increase the mesh elements in the near wake (see Fig .4).

3.2 Mesh Sensitivity Test

The solid-fluid interaction region is the most critical area that must be treated with attention during mesh generation (i.e., the boundary layer region). In this study, the height of the first mesh element (y_p) near the wall is estimated using the inverse y^+ relationship given by:

$$y_p = \frac{y^+ \mu}{u_\tau \rho} \tag{1}$$

Where u_τ is the friction velocity defined by $u_\tau = \sqrt{\tau_w/\rho}$, and τ_w is the wall shear stress linked to the skin friction coefficient (C_f) as follows:

$$\tau_w = \frac{1}{2} C_f \rho U_\infty^2 \tag{2}$$

Here, y^+ is set to 1.0 in Eq. 1, and C_f has been calculated using the Schlichting correlation (Schlichting *et al.* 1960) given by:

$$C_f = [2\log_{10}(Re) - 0.65]^{-2.3} \tag{3}$$

where Re is the Reynolds number based on the radius of the blade R (i.e., $Re = \rho U_\infty R/\mu$).

Based on the first element height (y_p), 15 structured mesh layers have been created near the blade/nacelle walls for spatial resolution of the boundary layer.

A mesh sensitivity test has been carried out for the Blade configuration. The Rotor configuration was then given the same mesh parameters. Three mesh cases have been considered, representing coarse (2.3 million nodes), medium (5.1 million nodes) and fine mesh (12 million nodes).

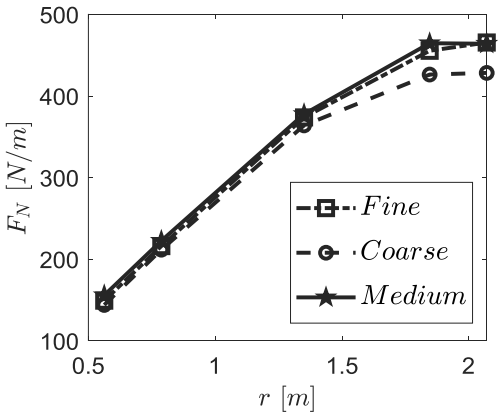

Fig. 5. Comparison of normal forces along the blade for TSR =6.7 using three mesh cases.

Figure 5 shows the comparison of the normal force distribution simulated at the design condition (i.e., TSR = 6.7). As indicated in Fig. 5, the results of the medium and fine meshes are very close to each other. While the results of the coarse mesh were far away, especially in the blade tip region. In addition, to properly examine the mesh effect, the mechanical

power for the three mesh cases has been computed and presented in the Table. 1.

As it can be seen in Table 1, the absolute error difference between the medium and fine meshes is less than 1%. Accordingly, the medium mesh has been used for the Blade configuration. For the Rotor configuration, the same mesh features were used.

For the two configurations (Blade and Rotor configurations), the average size of the elements in the rotating and stationary parts was 0.02 and 0.05 m, respectively. The Blade configuration mesh has around 5.1 million nodes, whereas the Rotor configuration mesh has 38 nodes.

Table 1 Mechanical power for the three meshes

Mesh case	Node number ($\times 10^6$)	Power (kW)	Absolute Error (%)
Coarse	2.314206	12.121	14.10
Medium	5.191501	15.066	06.76
Fine	12.305786	14.912	05.67

3.3 Mathematical Model

Steady-state numerical simulations of the flow around the MEXICO wind turbine were performed in this work for two configurations (Blade and Rotor configurations) using an incompressible finite volume CFD solver; ANSYS Fluent. The k-kl-ω (Walters and Cokljat 2008) transitional turbulence model was used to solve the RANS equations. This model is a low Reynolds model based on three transport equations, namely turbulent kinetic energy (k), laminar kinetic energy (kl), and the inverse turbulent time scale (ω). Since this model requires y^+ to be equal to or less than 1, Eqs. (1) to (3) are used to estimate the height of the first node near the wall. Figure 6 shows the distribution of y^+ at different blade sections, confirming that y^+ is always smaller than 1. Furthermore, the Multiple Reference Frame (MRF) approach has been used to allow the blades' rotation (Luo and Gosman 1994).

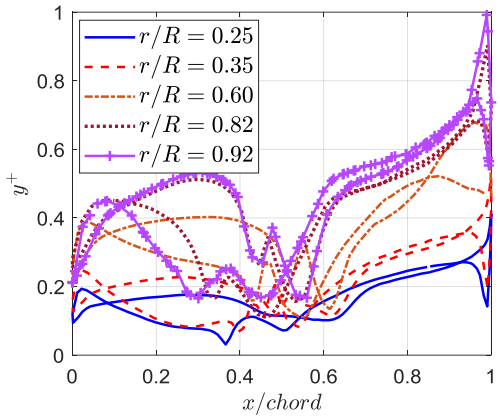

Fig. 6. y^+ distribution at different blade sections.

The flow variables are the three averaged velocity components, pressure, turbulent kinetic energy, laminar kinetic energy, and inverse turbulent time scale. The governing equations can be expressed using a general transport equation for a general variable ϕ as follows:

$$\vec{\nabla}.\left(\rho\vec{V}\phi\right) = \vec{\nabla}\cdot\left(\Gamma\,\vec{\nabla}\phi\right) + S_\phi \qquad (4)$$

In Eq. (4), the left term represents convection, the first right term represents diffusion. Γ is the diffusion coefficient, and S_ϕ is a source term. Table 2 summarizes the governing equations to be solved in the CFD solver.

In Table 2, G and Y are respectively the production and the dissipation of energy (for k, kl and ω), α_T is the turbulent scalar diffusivity. For further information about the k-kl-ω model, see (Walters and Cokljat 2008).

Table 2 Governing equations

Equation	ϕ	Γ	S_ϕ
Continuity	1	0	0
x- momentum	$\bar{u}$	μ	$-\frac{\partial \bar{p}}{\partial x}$
y- momentum	$\bar{v}$	μ	$-\frac{\partial \bar{p}}{\partial y}$
z- momentum	$\bar{w}$	μ	$-\frac{\partial \bar{p}}{\partial z} - \rho g$
Turbulent kinetic energy	k	ν	$G_k - Y_k$
Laminar kinetic energy	kl	$\mu + \rho\alpha_T$	$C_{kl} - Y_{kl}$
Inverse turbulent time scale	ω	$\mu + \rho\frac{\alpha_T}{1.17}$	$C_\omega - Y_\omega$

3.4 Boundary Conditions

The boundary conditions that have been used in this work can be summarized as follows:

(i) uniform axial velocity and low turbulence intensity at the inlet boundary.

(ii) Atmospheric pressure at the outlet boundary.

(iii) An interface technique was applied to separate rotating parts from stationary parts.

(iv) In the case of the Blade configuration, the remaining blades were calculated using periodic boundary conditions, taking advantage of the MEXICO rotor geometry's 120° symmetry.

(v) The no-slip condition implies that the flow velocity is zero on the blade/nacelle walls.

3.5 Numerical Simulation and Computational Time

In this study, the convective terms for all equations were discretized using the second order Upwind scheme and the diffusion terms are discretized using central differencing scheme.

All the steady-state simulations presented in this paper are computed by a parallel PC with 64 GB RAM and 6 x 3.31 GHz CPU.

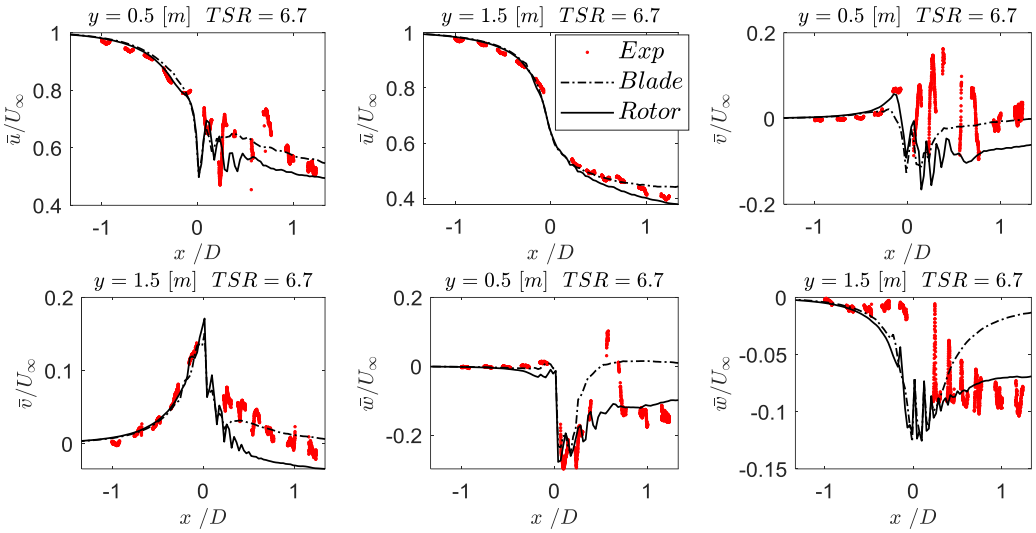

Fig. 7. Comparison between CFD simulations (blade alone and full rotor configurations) and PIV measurements of normalized velocity components along axial traverses y = +0.5 and y = +1.5m for TSR = 6.7.

To resolve the Pressure-Velocity coupling equations, the SIMPLE (Semi-Implicit Method for Pressure-Linked Equations) (Patankar 2018) and Coupled (ANSYS Fluent 2017) algorithms were compared for the Blade configuration, and it was found that the Coupled algorithm can accelerate the convergence of solutions and is more stable. The solutions converge with the SIMPLE algorithm for about 4500 iterations, and the computation time takes 3 days. On the other hand, when the Coupled algorithm is used, the solutions converge after 200 iterations, with a computation time of 22 hours. Therefore, the Coupled algorithm is recommended for this type of simulations (i.e., steady-state simulations of the flow around wind turbines). Noting that the Coupled algorithm resolves implicitly the continuity and the momentum equations.

4. RESULTS AND DISCUSSION

The flow around the MEXICO rotor is numerically simulated with three cases at axial wind velocities of 10 m/s (TSR = 10), 15 m/s (TSR = 6.7), and 24 m/s (TSR = 4) for the two studied configurations (without and with nacelle). The three averaged components of axial ($\bar{u}$), tangential ($\bar{v}$), and radial ($\bar{w}$) velocities in the near wake were computed and compared with PIV measurements to assess the influence of nacelle on the near wake.

As indicated in Fig. 3, the axial and radial velocities were extracted at the 9 o'clock position in the horizontal plane. The axial velocities were measured in two traverses' positions: inboard part (y = 0.5 m) and outboard part (y = 1.5 m) of the blade, and the radial velocities were measured upstream and downstream of the rotor, at the positions x = +0.3 m and x = -0.3 m respectively.

4.1 Axial Flow Behaviors

Let's begin with the axial flow behavior in the near wake. Figure 7 shows the distribution of the normalized velocities along the inboard (y = 0.5 m) and outboard (y = 1.5 m) traverses, computed and measured at the design condition (TSR = 6.7). Form the Fig.7, the PIV measurements indicated that the axial velocity profile ($\bar{u}$) in the outboard line (y = 1.5 m) begins with a constant value (free stream wind speed), then rapidly drops on the level of the rotor owing to blade rotation until it reaches a fixed value downstream of the rotor, where the velocity profile is stabilized. The prediction of this velocity induction is critical, particularly when investigating the interaction of turbines located in wind farms.

Because the wind speed was incoming in the axial direction, the radial ($\bar{v}$) and tangential ($\bar{w}$) velocity profiles began with zero value in the upstream of the rotor, and then, as a result of the variation in fluid velocity caused by the blades' rotation, the radial and tangential velocities began to gradually appear to have a maximum variation at the level of the rotor, and this variation disappeared progressively until it re-stabilized at zero in the downstream.

The simulation results were in good agreement with the PIV measurements for the two studied configurations (with and without nacelle). The difference in maximum and minimum absolute errors for the axial velocity component ($\bar{u}$) between the Blade and Rotor configurations was 6.2059% and 0.1889%, respectively. This means that taking nacelle geometry into account in CFD simulations can improve axial velocity prediction by around 6%.

The same fluid behavior was also noticed for the inboard line (y = 0.5 m) as indicated in Fig. 7. However, the flow is more complicated in this region due to the presence of the nacelle. Oscillations occur for all velocity components due to vortices generated by the nacelle geometry in the near wake region.

The difference in maximum and minimum absolute errors for the axial velocity component ($\bar{u}$) between the Blade and Rotor configurations, in this case, was 6.2059% and 0.1889%, respectively. The results showed that introducing the nacelle geometry into

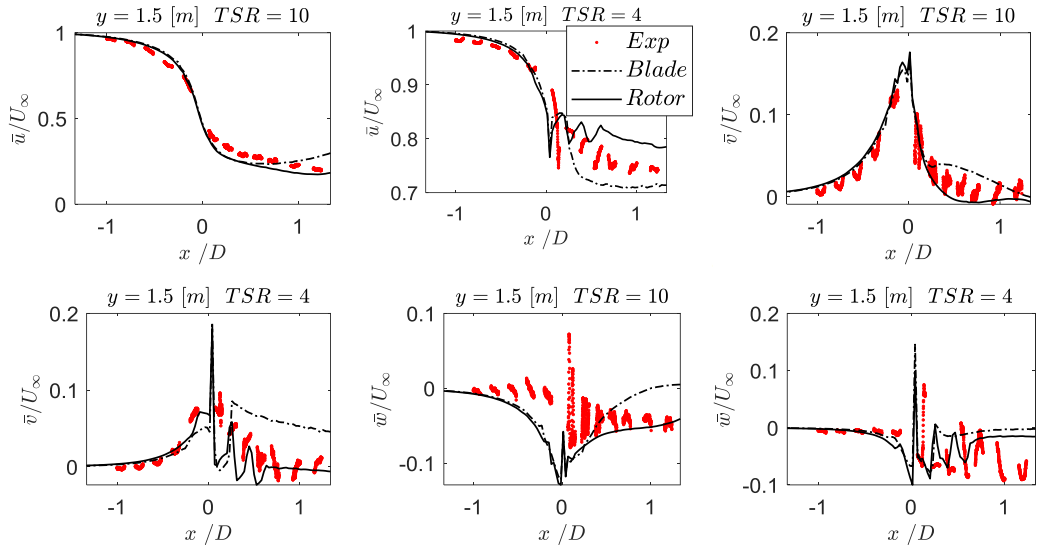

Fig. 8. Comparison between CFD simulations (blade alone and full rotor configurations) and PIV measurements of normalized velocity components along the axial traverse y = +1.5m for TSR = 10 and 4.

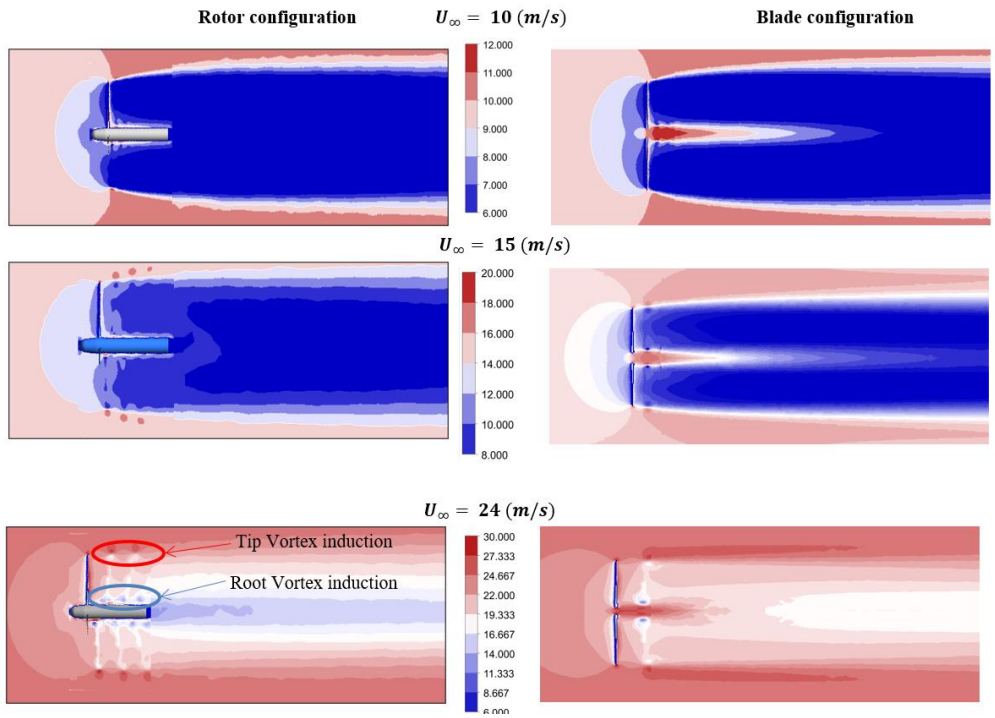

Fig. 9. Comparison of axial velocities contours extracted at x = 0m plan for the two studied configurations.

CFD improves near wake prediction by about 5%.

Since the inboard traverses are not available in MEXICO tests. Figure 8 shows only the velocity components normalized by the free wind speeds along the outboard line (y = 1.5 m) for the two off-design conditions (TSR = 4 and 10). For the lowest wind speed (TSR = 10), the two configurations agree well with the experimental data. The difference in absolute error between the two configurations does not exceed 1.1%. In the other hand, for the highest wind speed (TSR = 4), where the flow is separated, the maximum absolute error difference between the two configurations is greater than 15%. The presence of boundary layer separation on the nacelle and blade walls complicates the flow. The Rotor configuration results are in good agreement with the experimental data and closely follow the velocity oscillations downstream of the rotor.

The axial velocity contours for different wind speeds have been plotted in Fig. 9 to properly assess the fluid structure and behavior of the axial flow in the near wake. It can be seen that the flow's interaction

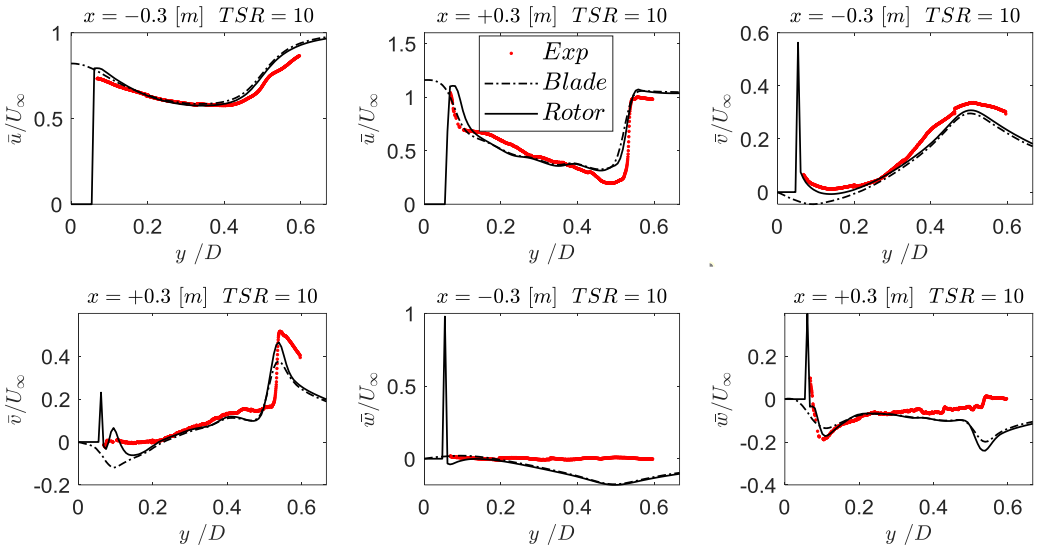

Fig. 10. Comparison between CFD simulations (blade alone and full rotor configurations) and PIV measurements of normalized velocity components along radial traverses x = +0.3 and x = -0.3 m for TSR = 10.

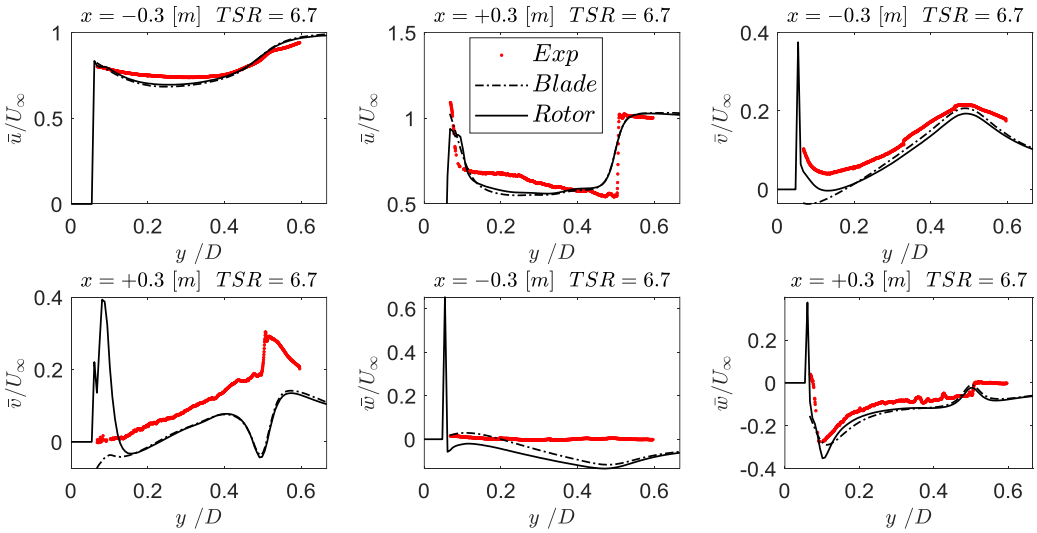

Fig. 11. Comparison between CFD simulations (blade alone and full rotor configurations) and PIV measurements of normalized velocity components along radial traverses x = +0.3 and x = -0.3 m for TSR = 6.7.

with the rotor reduces the velocity of the fluid downstream (i.e., the induction region), and this region decreases with the augmentation of wind speed for both configurations.

As shown in Fig. 9, the fluid is subjected to excessive acceleration in the root area of the blades in the case of the turbine without the nacelle. Previous research has observed this phenomenon (Guo *et al.* 2021; Zheng *et al.* 2018).

It can also be seen from Fig. 9 that, in addition to blade tip vortices, the presence of the nacelle creates root vortices near the nacelle wall and corrects the velocity induction behind the rotor, especially for design and high wind speeds. At low wind speeds, the prediction of wake flow fields was nearly identical for both configurations.

4.2 Radial Flow Behaviors

Following the comparison of axial flow, the emphasis is now on radial flow behavior. Figs. 10, 11, and 12 show the normalized velocity components at the upstream (x =-0.3 m) and downstream (x =+0.3 m) traverses near the rotor for both studied configurations (with and without the nacelle) for the three conditions TSR = 10, 6.7, and 4, respectively.

For the low wind speed (TSR = 10), as indicated in Fig. 10, the axial velocity ($\bar{u}$) decreases from the root to the tip of the blades due to the rotation of the blades for both upstream and downstream lines. After the fluid leaves the induction region, it returns to its initial velocity (free stream wind speed). Both configurations gave a good prediction of the width of the induction region. The greatest decrease in axial velocity for both numerical simulation and

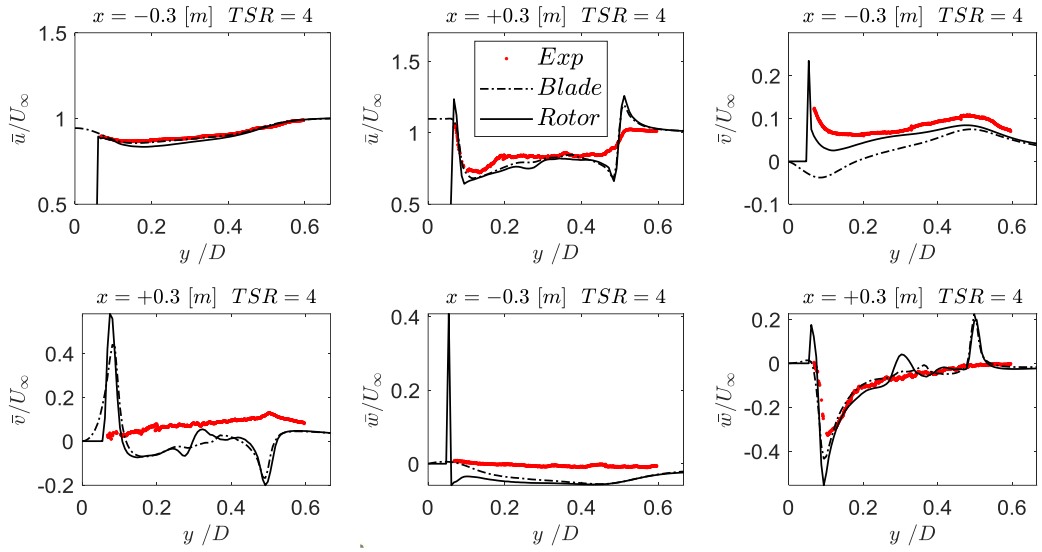

Fig. 12. Comparison between CFD simulations (blade alone and full rotor configurations) and PIV measurements of normalized velocity components along radial traverses x = +0.3 and x = -0.3 m for TSR = 4.

experimental measurements was detected at $y/D = 0.45$ and $y/D = 0.5$ for upstream and downstream lines, respectively. In addition, due to the conservation of mass, the flow is forced to change its direction at the rotor level, which leads to an increase in its radial velocity ($\bar{v}$) and a decrease in its tangential velocity ($\bar{w}$). Both configurations (with and without the nacelle) produced accurate radial velocity predictions. However, the tangential velocity is slightly underestimated, particularly at the blade tips. Indeed, this is due to the well-known weakness of RANS/URANS turbulence models as reported in previous studies (Micallef 2012; Sørensen *et al*. 2014; Thé and Yu 2017).

With the increase of wind speed, as indicated in Figs. 11 and 12, the point of greatest velocity decrease turns back toward the center of the rotor and its normalized magnitude decreases. The difference in prediction between the two configurations is more pronounced, especially at high wind speeds.

It can be seen from Figs. 10, 11 and 12 that, in the absence of the nacelle, the radial flow behavior is underpredicted at the tip and overpredicted at the root of the rotor. Therefore, the presence of the nacelle affects both tip and root flows.

The tip flow behavior refers to the separation resulting from the nacelle as indicated in the previous study done by (Akay *et al*. 2014). While the overprediction in the outer part of the blade is still unknown, it can be explained here that the presence of the nacelle causes large separation zones to reach the blade tip. This phenomenon will be demonstrated in the next section.

4.3 Flow Separation

As previously demonstrated by the results shown in the preceding sections, the presence of the nacelle improves the near wake prediction, especially at high wind speeds, while the nacelle effect can be neglected at low wind speeds. The purpose of this section is to figure out why the nacelle improves the near wake prediction and to reveal the physics behind the nacelle effect on the near wake under various attached and detached flow conditions.

Figs. 13 and 14 show the streamlines on the suction side of the blade (on the upper side downwind), as well as the streamline contours in the planes normal to the blade surface for the two studied configurations (with and without the nacelle), at five sections representing blade span locations of 0.25, 0.35, 0.60, 0.82, and 0.92.

It can be observed from Figs. 13 and 14 that, at low and medium wind speeds (TSR = 10 and 6.7), the streamlines are parallel to each other, and the flow remains attached to the whole of the suction side of the blade as well as to the upper and lower sections of the airfoils. However, due to vortex shedding in the blade's root, a slight radial component appears in this region for both configurations (with and without the nacelle). The results show that the angle of attack (angle between relative velocity direction and chord line) increases from tip to root of the blade in each case due to twist angle augmentation. Additionally, as the wind speed increases, this angle increases, and as a result, the separation appears at high wind speeds on the upper sections of airfoils (extrados) for both configurations (with and without the nacelle).

It can be seen from Fig. 13 that, at high wind speeds (TSR = 4), the presence of the nacelle causes a strong separation of the flow, and a recirculation bubble appears at the trailing edges of the entire blade, which reaches the rotor tip. Unlike in the case of the isolated blade, the flow separation and the recirculation bubble become weaker. This recirculation bubble, generated from the flow separation on the blade surface at high wind speeds, is the cause of the formation of the root and tip vorticities. The comparison indicated that the presence of the nacelle causes massive flow

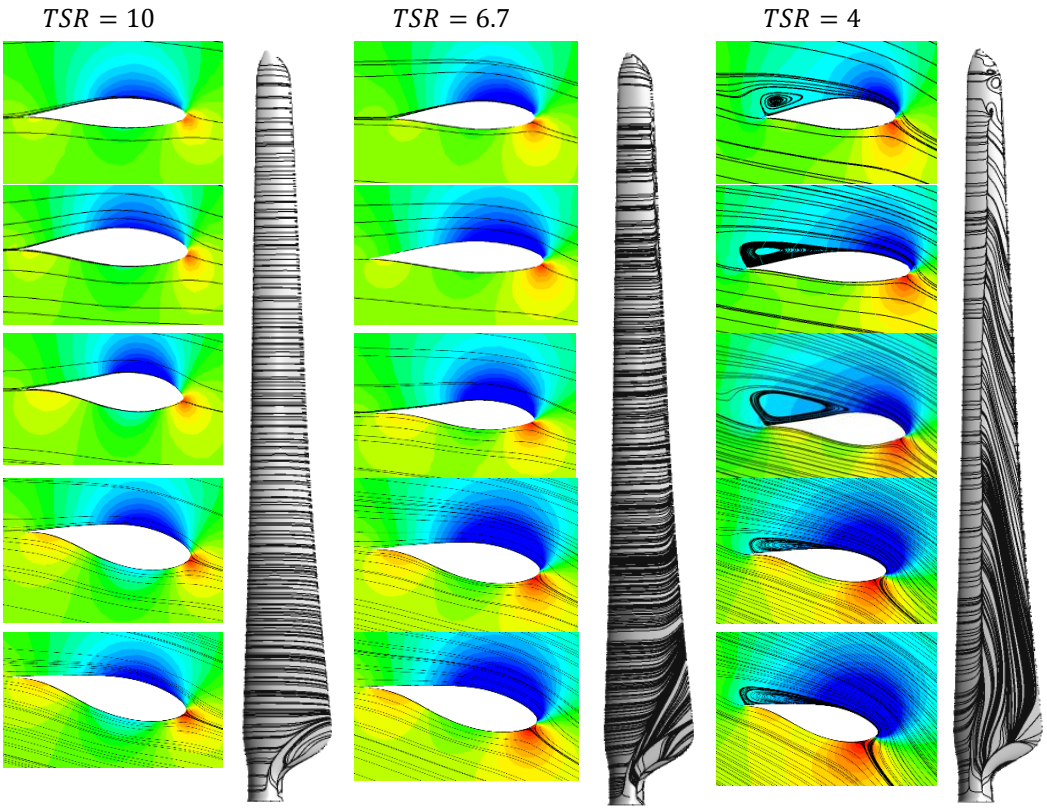

Fig. 13. Streamlines at the upper (downwind) side of the blade and streamline contours at five span-wise sections simulated for the Rotor configuration case (with the nacelle) for three TSR.

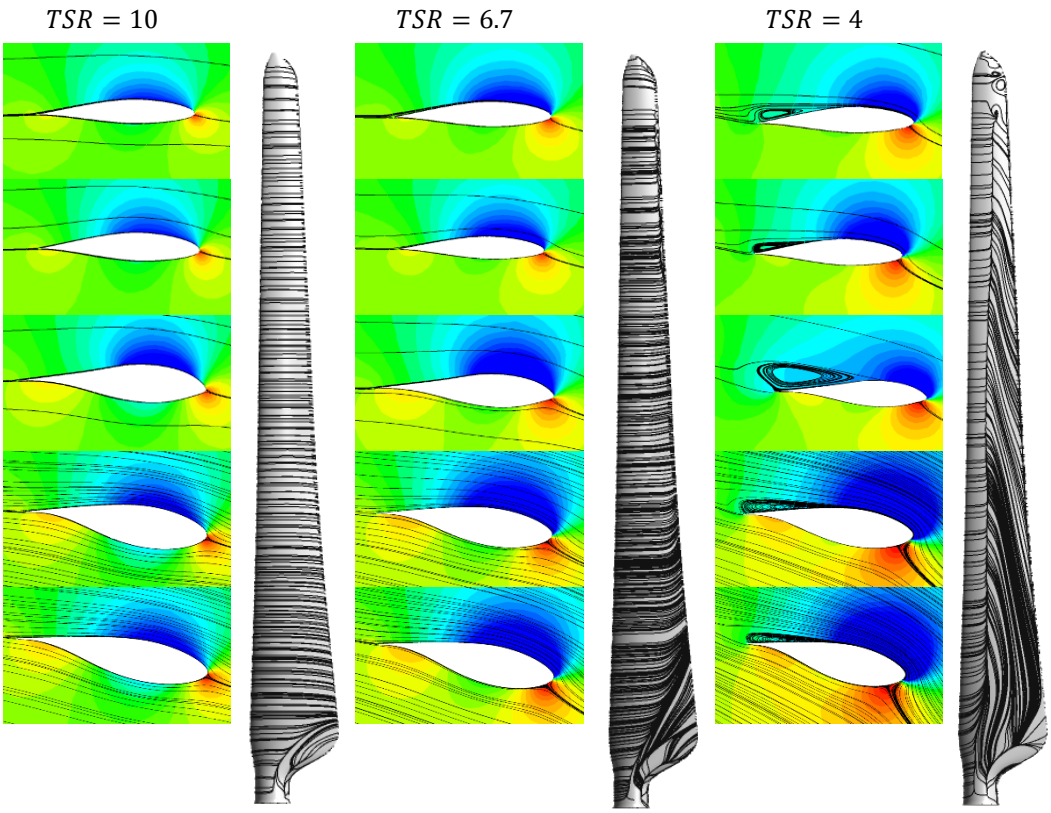

Fig. 14. Streamlines at the upper (downwind) side of the blade and streamline contours at five span-wise sections simulated for the Blade configuration case (without the nacelle) for three TSR.

separation on the blades, resulting in stronger vorticity and, as a result, reduced velocity in the near wake at high wind speeds. At low wind speeds, however, there is no significant difference in near wake predictions between the Blade and Rotor configurations because the flow is mostly attached and there are no vorticities. This explains the near wake overprediction previously observed in Fig.9 for the isolated blade configuration at high wind speeds.

5. CONCLUSION

The purpose of this work is to deeply study the physics of near wake flows downstream of wind turbines as well as to evaluate the near wake predictions with and without the nacelle. To achieve this objective, the full-geometry CFD approach has been used to simulate the steady-state flow around an experimental wind turbine, namely the MEXICO model. The transitional three-equation k-kl-ω turbulence model has been used to enclose the RANS equations. To assess the effect of the nacelle, two computational domains have been considered: (i) Rotor configuration including the whole rotor with the hub and nacelle; and (ii) Blade configuration representing only an isolated blade.

Three axial wind speeds, representing attached, design, and detached conditions, have been simulated. The velocity components in axial and radial lines are compared with the MEXICO measurements. Good agreements have been obtained for both configurations with and without the nacelle geometry. According to the obtained results, at low wind speed values, the nacelle geometry may enhance near wake numerical predictions by about 5%. At high wind speed values, however, the flow becomes more complicated, and the inclusion of the nacelle improves near wake predictions by increasing tip and root vortices near the wall. It has been shown that the rotor-nacelle interactions may improve the near wake predictions by up to 15% at high wind speeds, and the CFD results closely follow the velocity oscillations downstream of the rotor.

In addition to the effects of the nacelle that were concluded in previous studies, such as that the presence of the nacelle increases turbulence and turbulent kinetic energy and creates vortices in the root, new insights were addressed in this study, the most prominent of which are:

- At high tip speed ratios (or low wind speeds) where the flow is attached, the effect of the nacelle can be ignored.
- The effect of the nacelle is directly related to the tip speed ratio (or wind speed) and its main reason is the flow separation produced by the nacelle and the blades (together). The smaller the tip speed ratio (or higher the wind speed), the greater the separation in the blade.
- The flow separation is caused primarily by the detachment of the boundary layer at the trailing edges of the blade airfoils, and that is responsible for the formation of both root and tip vorticities.
- The presence of the nacelle enhances flow separation across the entire blade. At high wind speed values, the separation can reach the blade tip and intensify the tip vortices.
- The flow separation in the blade is less in the absence of the nacelle than in the presence of the nacelle, resulting in an overprediction of the velocity field behind the rotor. Therefore, it is recommended to use small nacelle diameters in order to reduce the flow separation at the blades and thus increase the velocity in the near wake and the output power of wind farms.

Finally, the main challenge remains evaluating how far the results of this work can be generalized by studying numerically and experimentally other wind turbine models of various scales in the future. In addition, future research should include unsteady simulations and POD (proper orthogonal decomposition) analyses to gain a better understanding of the near wake dynamics.

ACKNOWLEDGEMENTS

The data used in this paper were supplied by the consortium which carried out the EU FP5 project called MEXICO: "Model rotor EXperiments In COntrolled conditions," to which nine European partners contributed.

The support from Directorate-General for Scientific Research and Technological Development (DG-SRDT) of Algerian government i n the form of research grant is gratefully acknowledged.

We would like to express our heartfelt condolences to Pr. Christian Masson, the fourth author of this paper, who passed away recently.

REFERENCES

Abraham, A., T. Dasari and J. Hong (2019). Effect of turbine nacelle and tower on the near wake of a utility-scale wind turbine. *Journal of Wind Engineering and Industrial Aerodynamics* 193, 103981.

Akay, B., D. Micallef, C. J. S. Ferreira and G. J. van Bussel (2014). Effects of geometry and tip speed ratio on the HAWT blade's root flow. *Journal of Physics: Conference Series 555. IOP Publishing, 012002.*

ANSYS Fluent, A. (2017). ANSYS Fluent Documentation (version 18.1) *ANSYS Inc*.

Bartl, J. and L. Sætran (2016). *Experimental testing of axial induction based control strategies for wake control and wind farm optimization.* Journal of Physics: Conference Series 753. IOP Publishing, p. 032035.

Bastankhah, M. and F. Porté-Agel (2014). A new analytical model for wind-turbine wakes. *Renewable Energy* 70, 116-123.

Boorsma, K. and J. Schepers (2014). New MEXICO experiment. *Preliminary Overview with Initial Validation Technical Report ECN-E–14-048 ECN*.

Bouhelal, A., A. Smaili, O. Guerri and C. Masson (2018). Numerical investigation of turbulent flow around a recent horizontal axis wind Turbine using low and high Reynolds models. *Journal of Applied Fluid Mechanics* 11(1), 151-164.

Dahlberg, J., S. Frandsen, H. A. Madsen, I. Antoniou, T. Friis Pedersen, R. Hunter and H. Klug (1999). Is the nacelle mounted anemometer an acceptable option in performance testing?. *RISO-R-1114(EN)CONF-99031*, 51-55.

De Cillis, G., S. Cherubini, O. Semeraro, S. Leonardi and P. De Palma (2021). POD ‐ based analysis of a wind turbine wake under the influence of tower and nacelle. *Wind Energy* 24(6), 609-633.

Feng, J., W. Z. Shen and Y. Li (2018). An optimization framework for wind farm design in complex terrain. *Applied Sciences* 8(11), 2053.

Gao, Z., X. Feng, Z. Zhang, Z. Liu, X. Gao, L. Zhang, S. Li and Y. Li (2022). A brief discussion on offshore wind turbine hydrodynamics problem. *Journal of Hydrodynamics* 34(1), 15-30.

Gao, Z., Y. Li, T. Wang, W. Shen, X. Zangh, S. Pröbsting, D. Li and R. Li (2021). Modelling the nacelle wake of a horizontal-axis wind turbine under different yaw conditions. *Renewable Energy* 172, 263-275.

Guo, T., X. Guo, Z. Gao, S. Li, X. Zheng, X. Gao, R. Li, T. Wang, Y. Li and D. Li (2021). Nacelle and tower effect on a stand-alone wind turbine energy output—A discussion on field measurements of a small wind turbine. *Applied Energy* 303, 117590.

Hansen, M. O. L., J. N. Sørensen, S. Voutsinas, N. Sørensen and H. A. Madsen (2006). State of the art in wind turbine aerodynamics and aeroelasticity. *Progress in Aerospace Sciences* 42(4), 285-330.

Luo, J., R. Issa and A. Gosman (1994). Prediction of impeller-induced flow in mixing vessels using multiple frames of reference. *8th European conference on mixing*. Institute of Chemical Engineers Symposium Series. p. 549-556.

Madsen, H. A. and F. Rasmussen (2004). A near wake model for trailing vorticity compared with the blade element momentum theory. *Wind Energy: An International Journal for Progress and Applications in Wind Power Conversion Technology* 7(4), 325-341.

Masson, C. and A. Smaili (2006). Numerical study of turbulent flow around a wind turbine nacelle. *Wind Energy: An International Journal for Progress and Applications in Wind Power Conversion Technology* 9(3), 281-298.

Masson, C., A. Smaïli and C. Leclerc (2001). Aerodynamic analysis of HAWTs operating in unsteady conditions. *Wind Energy: An International Journal for Progress and Applications in Wind Power Conversion Technology* 4(1), 1-22.

Micallef, D. (2012). *3D flows near a HAWT rotor: A dissection of blade and wake contributions*. Doctoral thesis. Delft University of Technology.

Micallef, D., G. van Bussel, C. S. Ferreira and T. Sant (2013). An investigation of radial velocities for a horizontal axis wind turbine in axial and yawed flows. *Wind Energy* 16(4), 529-544.

Patankar, S. V. (2018). *Numerical heat transfer and fluid flow*: CRC press.

Regodeseves, P. G. and C. S. Morros (2021). Numerical study on the aerodynamics of an experimental wind turbine: Influence of nacelle and tower on the blades and near-wake. *Energy Conversion and Management* 237, 114110.

Sanderse, B., S. Van der Pijl and B. Koren (2011). Review of computational fluid dynamics for wind turbine wake aerodynamics. *Wind Energy* 14(7), 799-819.

Santoni, C., K. Carrasquillo, I. Arenas ‐ Navarro and S. Leonardi (2017). Effect of tower and nacelle on the flow past a wind turbine. *Wind Energy* 20(12), 1927-1939.

Schepers, J., K. Boorsma, S. Gomez-Iradi, P. Schaffarczyk, H. A. Madsen, N. N. Sørensen, W. Shen, T. Lutuz, C. Schulz, I. Herraez and S. Schreck (2014). Final report of IEA Wind Task 29: Mexnext (Phase 2).

Schlichting, H., K. Gersten, E. Krause, H. Oertel and K. Mayes (1960). *Boundary-layer theory* (Vol. 7): Springer.

Smaili, A. and C. Masson (2004). On the rotor effects upon nacelle anemometry for wind turbines. *Wind Engineering* 28(6), 695-713.

Snel, H., J. Schepers and B. Montgomerie (2007). The MEXICO project (Model Experiments in Controlled Conditions): The database and first results of data processing and interpretation. *Journal of Physics: Conference Series 75. IOP Publishing, p. 01201*.

Sørensen, J., W. Shen and X. Munduate (1998). Analysis of wake states by a full ‐ field

actuator disc model. *Wind Energy: An International Journal for Progress and Applications in Wind Power Conversion Technology* 1(2), 73-88.

Sørensen, N. N., A. Bechmann, P. E. Réthoré and F. Zahle (2014). Near wake Reynolds‐averaged Navier‐Stokes predictions of the wake behind the MEXICO rotor in axial and yawed flow conditions. *Wind Energy* 17(1), 75-86.

Sørensen, N. N., J. Michelsen and S. Schreck (2002). Navier–Stokes predictions of the NREL phase VI rotor in the NASA Ames 80 ft× 120 ft wind tunnel. *Wind Energy: An International Journal for Progress and Applications in Wind Power Conversion Technology* 5(2‐3), 151-169.

Sørensen, N. N., F. Zahle, K. Boorsma and G. Schepers (2016). CFD computations of the second round of MEXICO rotor measurements. *Journal of Physics: Conference Series 753. IOP Publishing, p. 022054.*

Tescione, G., C. S. Ferreira and G. Van Bussel (2016). Analysis of a free vortex wake model for the study of the rotor and near wake flow of a vertical axis wind turbine. *Renewable Energy* 87, 552-563.

Thé, J. and H. Yu (2017). A Critical Review on the Simulations of Wind Turbine Aerodynamics Focusing on Hybrid RANS-LES Methods. *Energy* 138(1), 257-289.

Thomsen, K., H. A. Madsen, G. C. Larsen and T. J. Larsen (2007). Comparison of methods for load simulation for wind turbines operating in wake. *Journal of Physics: Conference Series 75. IOP Publishing, p. 012072.*

Walters, D. K. and D. Cokljat (2008). A three-equation eddy-viscosity model for Reynolds-averaged Navier–Stokes simulations of transitional flow. *Journal of Fluids Engineering* 130(12).

Weihing, P., T. Wegmann, T. Lutz, E. Krämer, T. Kühn and A. Altmikus (2018). Numerical analyses and optimizations on the flow in the nacelle region of a wind turbine. *Wind Energy Science* 3(2), 503-531.

Zahle, F. and N. N. Sørensen (2008). Overset grid flow simulation on a modern wind turbine. *AIAA paper* 6727, 2008.

Zheng, Z., Z. Gao, D. Li, R. Li, Y. Li, Q. Hu and W. Hu (2018). Interaction between the atmospheric boundary layer and a stand-alone wind turbine in Gansu—Part II: Numerical analysis. *SCIENCE CHINA Physics, Mechanics & Astronomy* 61(9), 1-10.

Zhu, X., C. Sun, H. Ouyang and Z. Du (2022). Numerical investigation of the effect of towers and nacelles on the near wake of a horizontal-axis wind turbine model. *Energy* 238, 121782.